Development of Bacteriochlorophyll *a*-Based Near-Infrared Photosensitizers Conjugated to Gold Nanoparticles for Photodynamic Therapy of Cancer

I. V. Pantiushenko[1], P. G. Rudakovskaya[2,3], A. V. Starovoytova[4], A. A. Mikhaylovskaya[4], M. A. Abakumov[5], M. A. Kaplan[4], A. A. Tsygankov[6], A. G. Majouga[2,3], M. A. Grin[1]*, and A. F. Mironov[1]

[1]*Lomonosov Moscow State University of Fine Chemical Technologies, 119571 Moscow, Russia; E-mail: michael_grin@mail.ru*
[2]*Lomonosov Moscow State University, 119991 Moscow, Russia; E-mail: alexander.majouga@gmail.com*
[3]*National University of Science and Technology MISiS, 119991 Moscow, Russia*
[4]*Cyb Scientific Research Center of Radiology, Hertsen Federal Medical Research Center, Ministry of Health*
of the Russian Federation, 249036 Obninsk, Kaluga Region, Russia; E-mail: kaplan@mrrc.obninsk.ru
[5]*Pirogov Russian National Research Medical University, Department of Medical Nanobiotechnology,*
117997 Moscow, Russia; E-mail: abakumov88@gmail.com
[6]*Institute of Basic Biological Problems, Russian Academy of Sciences,*
142290 Pushchino, Moscow Region, Russia; E-mail: ttt-01@rambler.ru

Abstract—We report the synthesis and characterization of a new sulfur-containing derivative of bacteriochlorophyll *a*. The latter was isolated from biomass of the nonsulfur purple bacterium *Rhodobacter capsulatus* strain B10. The developed photosensitizer is *N*-aminobacteriopurpurinimide with an exocyclic amino group acylated with a lipoic acid moiety, which is a biogenic substance that acts as a cofactor of the pyruvate dehydrogenase and α-ketoglutarate dehydrogenase complexes in the body. The disulfide moiety of lipoic acid confers the compound aurophilicity, thus allowing its conjugation with gold nanoparticles (NP–Au) via S–Au bonds. The shape and the size of the resulting nanoconjugate with immobilized photosensitizer (PS–Au) were assessed by dynamic light scattering and transmission electron microscopy. The conjugated nanoparticles are spherical with hydrodynamic diameter of 100-110 nm. The PS–Au conjugate absorbs light at 824 nm and emits strong fluorescence at 830 nm, which allowed *in vivo* study of its dynamic biodistribution in rats bearing sarcoma M-1. Compared to the free photosensitizer, PS loaded on the gold nanoparticles (PS–Au) showed extended circulation time in the blood and enhanced tumor uptake due to nonspecific passive targeting when the drug accumulates in tumor sites through the leaky tumor neovasculature and does not return to the circulation.

DOI: 10.1134/S0006297915060103

Key words: bacteriochlorophyll *a*, bacteriopurpurinimide, photosensitizers, photodynamic therapy, lipoic acid, gold nanoparticles, sarcoma M-1

Significant advances have been made improving the diagnosis and treatment of cancer. Still, the main current treatment options, i.e. surgical treatment, chemotherapy, and radiation therapy often suffer from severe adverse side effects and/or are not effective for all patients. However,

the last two decades have brought enormous progress in development of alternative therapeutic approaches, including photodynamic therapy (PDT) that combines three essential components: photosensitizer (PS), light, and oxygen to generate cytotoxic singlet oxygen [1-3]. Destruction of tumor tissue results from direct photoinduced cytotoxic effect in the cells, indirect vascular shutdown of the blood vessels surrounding the diseased tissue, and by invoking an immune response [4-6].

PDT is minimally invasive, can selectively destroy malignant tissues, and due to low toxicity of used PS it is

---

Abbreviations: BChl *a*, bacteriochlorophyll *a*; DLS, dynamic light scattering; NP-Au, gold nanoparticles; PDT, photodynamic therapy; PS, photosensitizer; PS–Au, gold nanoparticles with immobilized photosensitizer.
* To whom correspondence should be addressed.

a relatively benign procedure with minimal local and systemic side effects.

However, the technique has its limitations, i.e. PDT efficacy strongly depends on the depth of penetration of light into tissue. Another limitation is a relatively low selectivity of accumulation of PS in the tumor tissue characteristic of classical photosensitizers in clinical PDT [7, 8].

The photosensitizers most commonly employed for therapeutic applications and those explored in preclinical and clinical studies belong to different families (porphyrins and their metallocomplexes, chlorins, benzoporphyrins, phthalocyanines, etc.). Of particular interest is a group of naturally occurring chlorophylls and their derivatives having strong light absorption in the red and near IR spectral region as their therapeutic absorption window between about 660-800 nm enables ablation of tumors that cannot be accessed with PS absorbing at shorter wavelengths. Light of such wavelength penetrates into tissue to the depth of more than 20 mm, allowing treatment of deep-seated and pigmented tumors [9, 10].

The choice of natural pigments to be used for synthesis of new PS is influenced by several factors, including their natural occurrence, strong long-wavelength absorption, convenient substitution on side-chain functional groups, and structural similarity with endogenous porphyrins, which is thought to ensure low toxicity of PS and its rapid elimination from the body.

Unfortunately, due to high hydrophobicity, low chemical and photostability, limited tumor uptake of chlorins and bacteriochlorins, efforts are currently underway to modify them further in a way to enhance their photophysical properties, reach higher solubility in aqueous medium and polar solvents, and improve tumor affinity [11-15].

Use of gold nanoparticles (NP-Au) functionalized with PS is a promising approach to improve PDT drug delivery. Gold nanoparticles and gold nanoparticle conjugates possess a unique combination of properties. Gold nanoparticles are well known for chemical inertness and have minimal toxicity. They exhibit excellent optical and electronic properties, and their size can be tuned with characteristically large surface-to-volume ratios. The gold nanoparticle surface is one of the most stable and easily functionalized platforms for molecular conjugation.

Importantly, NP-Au can show increased binding affinity and targeting selectivity when functionalized with targeting groups, as well as tumor-selective uptake due to their size. They selectively accumulate in the tumor site through a passive targeting process due to the inherent leaky tumor neovasculature, which enhances the permeability and retention of the nano-sized particles [16-18], either through active targeting to tumor sites promoted by conjugating receptor-specific moieties onto the nanoparticle surface to afford vector delivery of the photosensitizer into the cell by receptor-mediated endocytosis or via specific receptors on cell membranes. Depending on the form, size, and functionalization, gold nanoparticles can be endocytosed or they attach to the outer leaflet of the membrane [19-21].

Recent reports have shown successful use of gold nanoparticles as a highly efficient drug vector for chemotherapy [22, 23] and PDT drug delivery [24-26]. However, combining photodynamic therapy with another therapeutic modality is still encouraged for cancer therapy because injection dose of the photosensitizer can be reduced to avoid potential side effects. Thus, the application potential of PDT can benefit from the combination with other therapeutic modalities such as radiation therapy [27, 28] and local hyperthermia treatment [29-31].

It is believed that combination gold nanoparticle-aided PDT and radiation therapy is can considerably improve the therapeutic effect using lower light and drug doses, also enabling effective treatment of radioresistant tumors. On irradiation with monoenergetic 100-keV X-rays, sensitized gold nanoparticles release photoelectrons. The range of these electrons is very short relative to photons, and a pronounced energy is deposited in cells containing gold nanoparticles or in direct proximity to gold atoms, producing a significantly increased apoptotic and dose-enhancing effects versus the radiation alone.

Another promising strategy for cancer treatment is the combination of gold nanoparticle-aided PDT and laser-induced photothermal treatment of tumors. Gold nanoparticles exhibit a remarkable visible absorption peak, which is related to the collective oscillation of conduction electrons inside the nanoparticles, known as localized surface plasmon resonance. The wavelength of light that excites resonance is absorbed and scattered by the nanostructure. Strong light absorption at the resonant wavelength enables gold nanostructures to generate a sufficient amount of heat by converting incident light into heat efficiently. This gold nanostructure-mediated photothermal heating can be further utilized to kill malignant cells, which is called photothermal therapy. By changing the shape and the dimension of the gold nanoparticles, the resonance wavelength can be tuned to obtain particles with controlled optical properties of nanoparticle-based agents that can generate heat efficiently by near IR light are more favorable for localized photothermal therapy.

Irradiation of a tumor by laser radiation with appropriate absorption wavelength of gold nanoparticles can cause local tumor hyperthermia. Selective accumulation of NP-Au in a tumor generates a strong temperature gradient between tumor and surrounding tissue, thus localizing damage to malignant cells.

Here we report the synthesis of an aurophylic bacteriochlorophyll *a* (BChl *a*) based photosensitizer that was covalently conjugated to NP-Au, its spectroscopic and photophysical characterization, and evaluation of PDT activity.

MATERIALS AND METHODS

The commercially available reagents, i.e. hydrazine hydrate solution (Merck, Germany), α-lipoic acid (Sigma-Aldrich, USA), Cremophor ELP (BASF, Germany), as well as domestic products were used as received. All solvents were purified and prepared using standard procedures. Bacteriopurpurin was derived from BChl *a* by the procedure developed at the Moscow State University of Fine Chemical Technologies, Department of Chemistry and Technology of Biologically Active Compounds [32].

TLC was performed on plates pre-coated with Kieselgel 60 F_{254} silica gel (Merck) using methylene chloride as a solvent. NMR spectra were recorded with a Bruker DPX-300 (Germany) instrument at 300 MHz. MALDI mass spectra were acquired on a Bruker Ultraflex TOF/TOF mass spectrometer (Germany) using 2,5-dihydroxybenzoic acid (DHB) as the MALDI matrix. UV-Vis absorption spectra were measured with an Ultrospec 2100 Pro (GE Healthcare, USA) spectrophotometer using standard 10 mm quartz cuvettes. All spectroscopic analyses were performed at 25°C. Centrifugation was performed with an Elmi Skyline CM50 centrifuge (ELMI, Latvia). Nanoparticle size characterization was performed using dynamic light scattering (DLS) on a ZetasizerNanoZS system (Malvern Instruments Ltd., UK) at backscattering angle $\theta = 173°$ with a He-Ne laser (633 nm, 5 mV). Transmission electron microscopy (TEM) images were acquired on a JEOLJEM-2100F/Cs/ GIF field-emission transmission electron microscope (200 kV, 0.8 Å). An IVIS Spectrum-CT system was used for *in vivo* fluorescence imaging of rats.

N-Aminobacteriopurpurinimide with attached lipoic acid moiety (PS) 4. A solution of *N*-aminobacteriopurpurinimide **3** (30 mg, 0.048 mmol) in methylene chloride (5 ml) was supplemented with α-lipoic acid (20 mg, 0.096 mmol) and N-carboethoxy-2-ethoxy-1,2-dihydroquinoline (12 mg, 0.048 mmol). The reaction mixture was stirred at room temperature for 36 h. The course of the reaction was followed using TLC and spectrophotometry. Then the reaction mixture was diluted with 150 ml distilled water and extracted with methylene chloride to full decolorization of the organic layer (3×30 ml). The combined extracts were dried over anhydrous sodium sulfate and concentrated with a rotary evaporator. The residue was chromatographed on silica eluting with CH_2Cl_2–CH_3OH (50 : 1 v/v).

Yield of PS **4** was 65%. ^1H NMR (300 MHz, CDCl$_3$, 50°C) δ, ppm: 9.10 (s, 10-H), 8.75 (s, 5-H), 8.50 (s, 20-H), 5.25 (m, 17-H), 4.33 (m, 18-H, 7-H), 4.1 (m, 8-H), 3.68 (s, 12-CH$_3$), 3.60 (d, $J = 5.1$ Hz, 4H, -CH$\underline{CH_2}$S-), 3.55 (s, 17^5-CH$_3$), 3.50 (s, 2-CH$_3$), 3.40-3.60 (1H, -CH$_2$$\underline{CH}$S–S), 3.18 (s, 3^2-CH$_3$), 3.05-3.12 (2H, -$\underline{CH_2}$S–S-), 2.75 (m, 8^1-CH$_2$), 2.42-2.50 (4H, -S–SCH$\underline{CH_2}CH_2CH_2$-, -S–SCH$\underline{CH_2}$-), 2.4 (m, 17^2-CH$_2$), 2.30 (t, $J = 6.7$ Hz, 2H, -$\underline{CH_2}$C(O)), 2.1 (m, 17^1-CH$_2$), 1.85 (d, $J = 7$ Hz, 7-CH$_3$), 1.71-1.93 (2H, -$\underline{CH_2}$CH$_2$CH$_2$C(O)), 1.70 (d, $J = 8$ Hz, 18-CH$_3$), 1.60-1.68 (2H, -$\underline{CH_2}$CH$_2$C(O)), 1.12 (t, $J = 7$ Hz, 8^2-CH$_3$), −0.25 (s, NH), −0.5 (s, NH).

MALDI, *m/z*: 799 (M$^+$).

UV-VIS (H$_2$O/Cremophor 4%) λ_{max}, nm: 365, 415 (Soret), 551 and 824 (relative intensity 1 : 0.68 : 0.39 : 0.92).

Preparation of aqueous micellar dispersion of *N*-aminobacteriopurpurinimide bearing lipoic acid moiety (PS) 4. A solution of PS **4** (10 mg) in methylene chloride (3 ml) was added periodically in 0.5 ml portions at 8-10 min intervals to 4% Cremophor in deionized water (10 ml). Methylene chloride was then removed by evaporation under argon in a thermostat-controlled water bath at 40°C. The resulting aqueous emulsion containing PS **4** was sterilized by filtration through a 0.4 μm Millipore (USA) filters with subsequent correction of the filtrate concentration by dilution with deionized water.

Immobilization of PS 4 methyl ether on gold nanoparticles (NP-Au). A solution of PS **4** was added to aqueous solution of NP-Au (1 mg PS **4** per 10 ml of solution of NP-Au) with vigorous stirring. The reaction mixture was allowed to stir for 24 h, then the resulting solution was centrifuged at 15*g* for 30 min, supernatant containing unreacted PS **4** was decanted, and precipitate containing PS **4** conjugated to gold nanoparticles (PS−Au) **5** was re-dispersed in 4% aqueous Cremophor.

Measurement of loading ratio of gold nanoparticles. The amount of immobilized PS was determined from the difference between the concentration of its initial solution and the concentration of supernatant decanted after centrifugation of PS−Au. Concentrations of free PS in the initial solution and PS conjugated to gold nanoparticles were calculated based on measured intensities of the long-wavelength band Q$_2$ in the electronic absorption spectrum before and after immobilization and the molar extinction coefficient of *N*-aminobacteriopurpurinimide bearing lipoic acid moiety. PS loading is characterized by the PS/NP-Au ratio.

Preparation of tumor-bearing laboratory animals. Tumor implanted in rat was used as donor tissue 14 days post implantation. Carrier rats were anesthetized with chloroform, then the tumor was excised and the capsule and necrotic tissue were removed. Donor tumor was minced in Hanks' solution into small pieces ((0.15-$0.25)\cdot10^{-3}$ cm^3) and inserted subcutaneously in the left hind leg of recipient rats. The recipient rats were treated starting on day 10-14 post transplantation after the tumors reached sufficient size.

Dynamics of *in vivo* PS and PS−Au accumulation in tumor. Dynamics of PS and PS−Au accumulation in tumor was assessed by local fluorescence spectroscopy with a Lesa-6 (Biospec, Russia) spectrometric system. Fluorescence was excited by 633 nm radiation from He-Ne laser (2 mW). Laser energy density delivered to the tissue surface per pulse was less than 1 J/cm^2, which is far
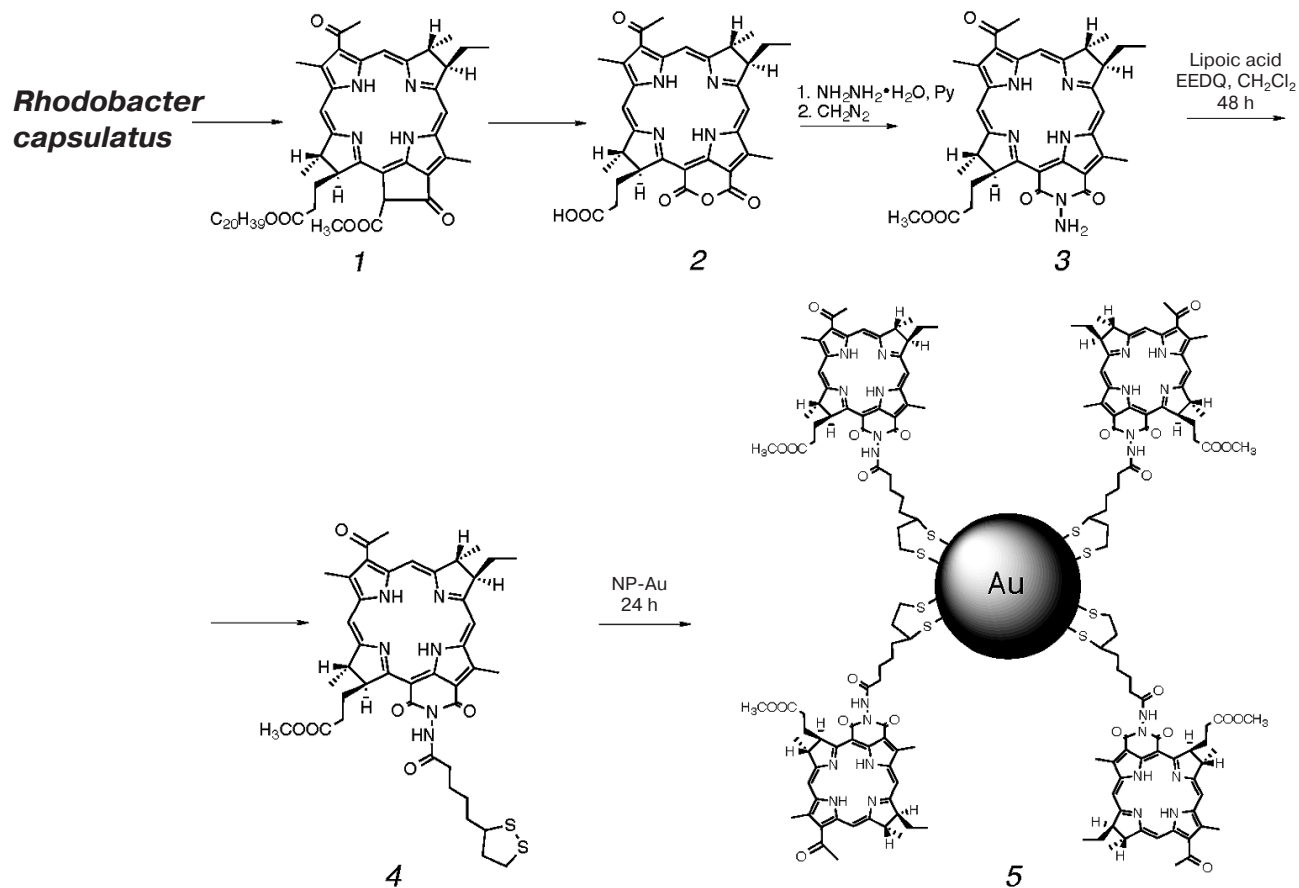
Synthesis of *N*-aminobacteriopurpurinimide-based photosensitizer conjugated to gold nanoparticles (PS−Au, **5**)

Scheme
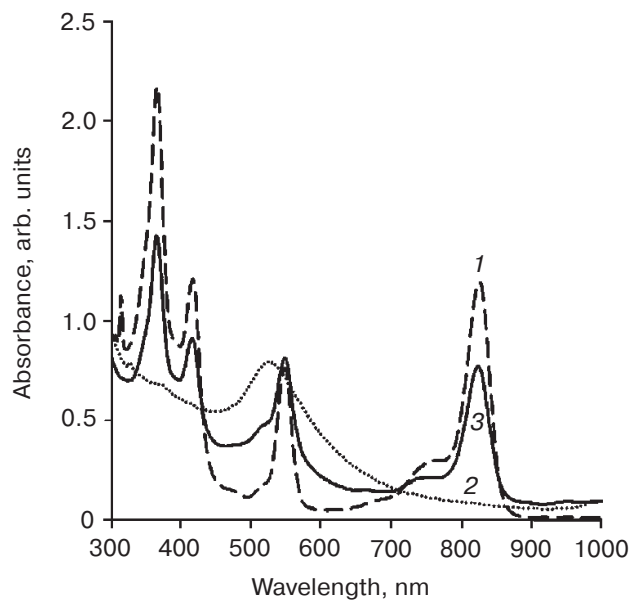
Fig. 1. Electronic absorption spectrum of micellar aqueous-Cremophor dispersion of the photosensitizer, PS (*1*), gold nanoparticles, NP-Au (*2*), and micellar aqueous-Cremophor dispersion of the photosensitizer conjugated to gold nanoparticles, PS−Au (*3*).
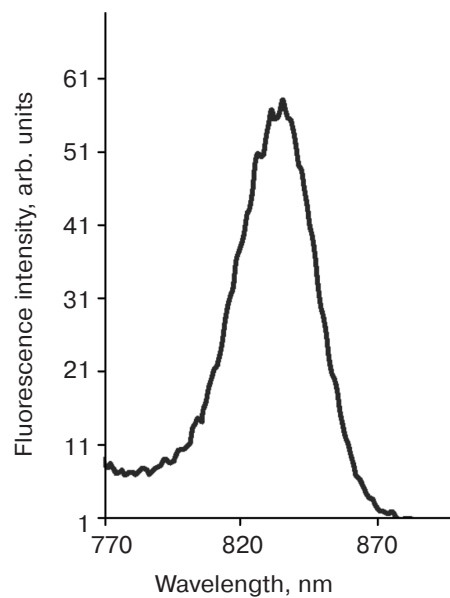
Fig. 2. Fluorescence emission spectrum of micellar aqueous-Cremophor dispersion of the photosensitizer conjugated to gold nanoparticles, PS−Au (540 nm excitation).

beyond the dose capable of inducing irreversible tissue damage unwelcome for diagnostic tests. Before treatment, the tumor region on the rat leg was depilated, also depilated was a small area (visually undamaged tissue) of the other hind limb.

Fluorescence was measured using right-angle illumination and collection geometry, using illumination with single-fiber quartz probes with a tip of the distal end in direct tissue surface contact. The acquisition time for fluorescence measurements (exposure time) was in the range
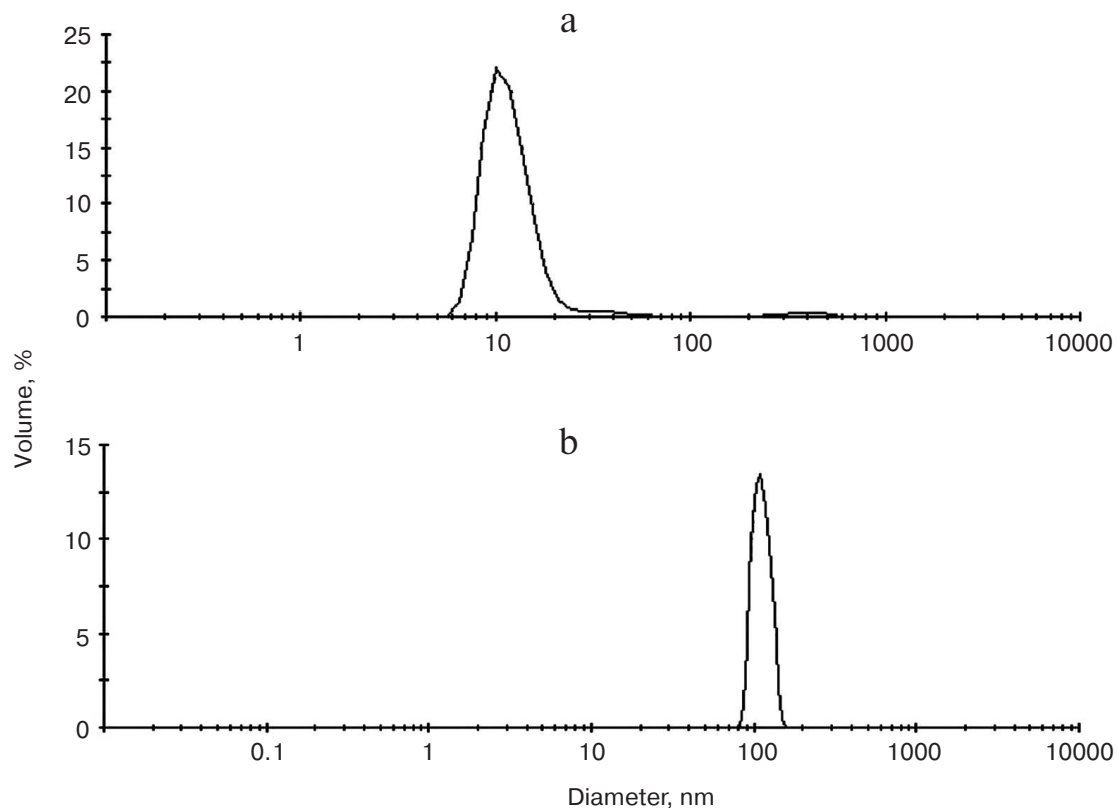

Fig. 3. Size distribution (calculated from DLS measurement) of unloaded gold nanoparticles (a) and gold nanoparticles with immobilized photosensitizer, PS−Au (b).
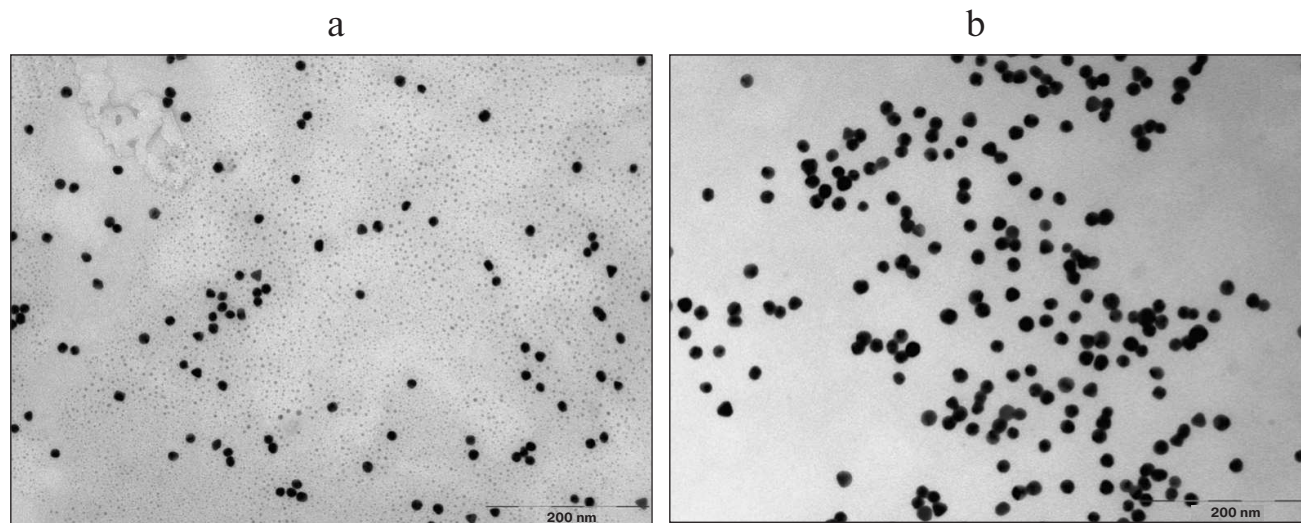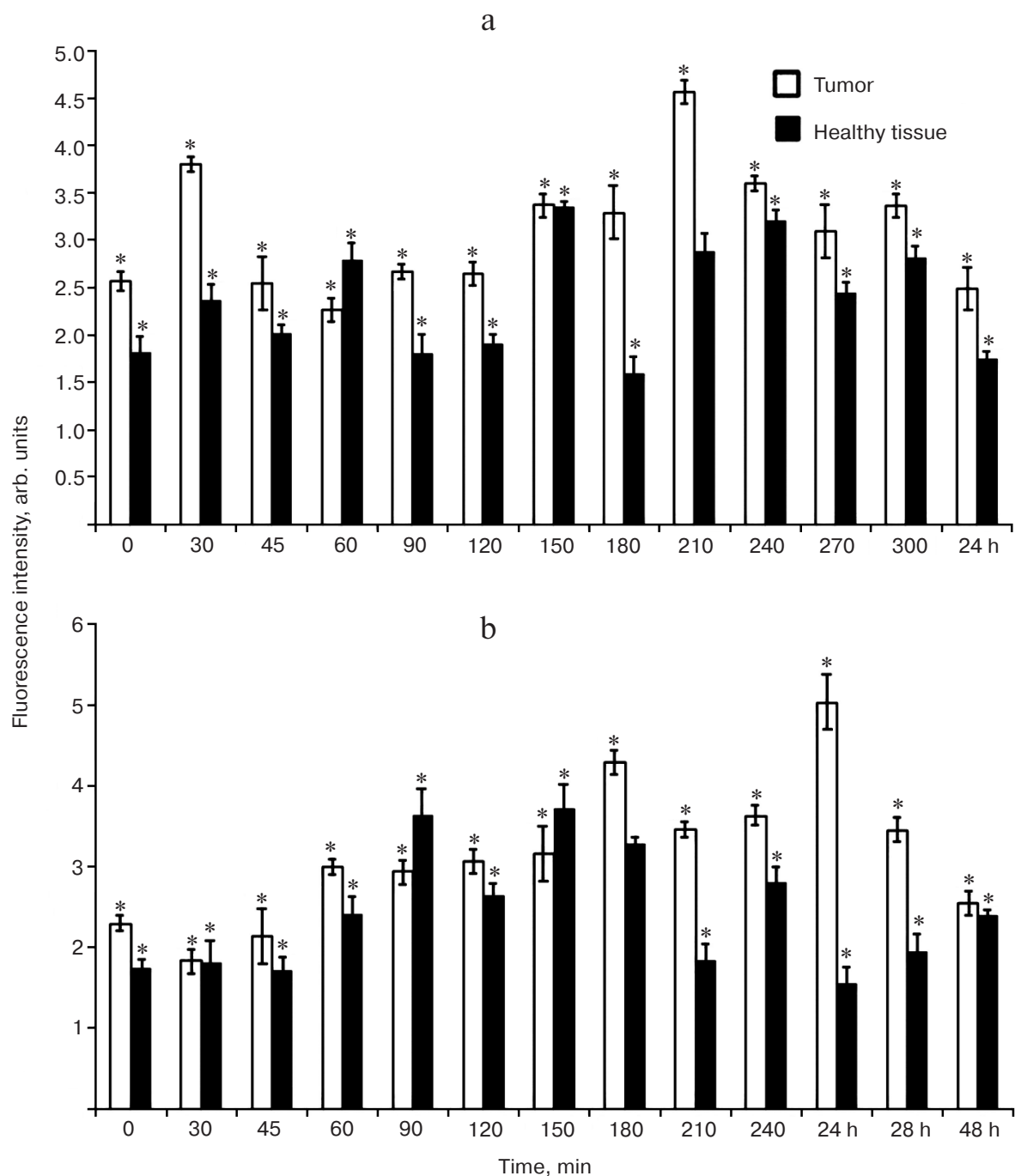

Fig. 4. TEM images of unloaded gold nanoparticles (a) and gold nanoparticles with immobilized photosensitizer, PS−Au (b).

Fig. 5. Accumulation kinetics of free and loaded on NP-Au photosensitizer (PS **4** (a) and PS−Au **5** (b), respectively) in tumor (rat sarcoma M-1) based on measured normalized fluorescence in tumor tissue over 5 sec to 48 h post-injection period (injection dose 2.5 mg/kg). Each value is the mean of three independent experiments; * $p < 0.05$ (95% confidence).

of 1-2 sec. The fluorescence emission spectra per site acquired from the tissue of tumor center and periphery and from visually undamaged tissue were evaluated in terms of line shape and intensity (signal amplitude). Then normalized fluorescence (NF) was determined as S_2/S_1, the ratio of areas under curves in fluorescence spectrum and backscatter spectrum, respectively. Selectivity of the PS accumulation in tumor compared to healthy tissue was estimated from the fluorescence contrast (FC) index − a ratio of S_2/S_1 value (averaged in animals' group) for tumor to the averaged S_2/S_1 value for healthy tissue. The output power of the optic fiber was measured with a spherical dosimeter. PDT treatment was performed using a Latus (Poluprovodnikovye Pribory, Russia) laser system.

Irradiance was determined as output power of a fiber-optic probe per illumination area: $Ps = P/S$, where Ps is irradiance (W/cm^2), P is output power of the optic fiber (W), and S is illumination area (cm^2). Illumination area was adjusted to incorporate, apart from the tumor site, the surrounding (peripheral) undamaged tissue (focused spot size 3-5 mm). The exposure time was found from the preset energy density required to be delivered to tumor and the calculated irradiance: $T = E/Ps$, where T is the exposure time (sec), E is the energy density (J/cm^2), and Ps is irradiance (W/cm^2).

***In vivo* fluorescence imaging of laboratory animals.** Rats were anesthetized with inhalation of 2% isoflurane (Abbott, USA) in a mixture with air. The tested PS was administered intraperitoneally, 2.5 mg/kg. Fluorescence images were obtained using the IVIS Spectrum-CT (PerkinElmer, USA) optical imaging system at Pirogov Russian National Research Medical University, Department of Medical Nanobiotechnology. Fluorescence emission spectra were measured at 710 and 745 nm excitation over 780, 800, 820, and 840 nm emission wavelengths. To discriminate autofluorescence background
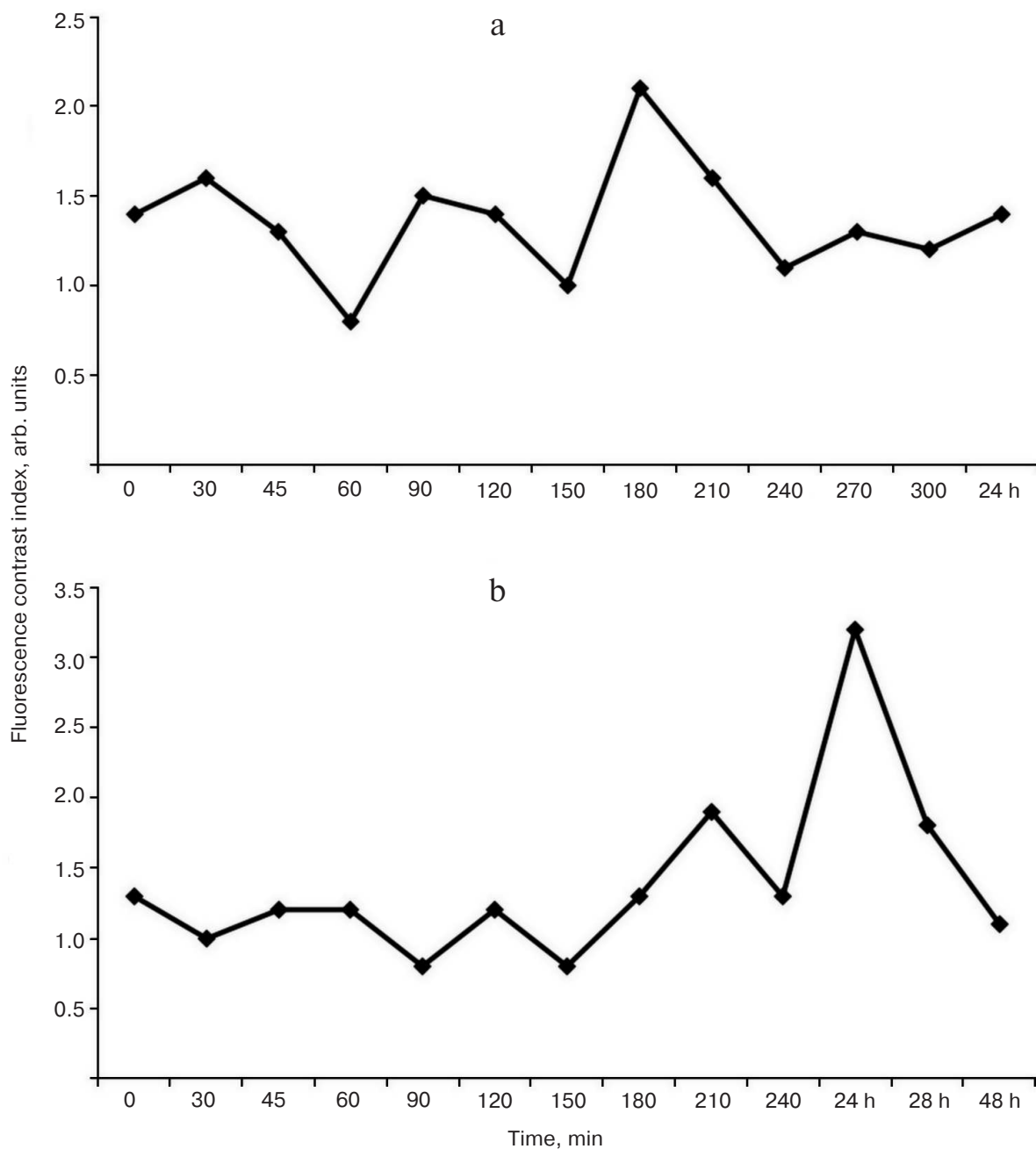
Fig. 6. Fluorescence contrast ratios of PS **4** (a) and PS–Au **5** (b) in tumor tissue (rat sarcoma M-1) over 5 sec to 24 h post-injection period (injection dose 2.5 mg/kg).

from the fluorescent signals of the fluorophore, we used LivingImage 4.4 (PerkinElmer, USA) software for deconvoluting absorption and scattering of the tissue from the measured fluorescence emission spectra. Fluorescence intensity was measured in photons/cm^2·sec.

Statistics. The data were analyzed by nonparametric statistics. Analysis of variance with non-parametric Mann−Whitney U-test was carried out using 95% confidence interval for difference between means in the Statistica 6.0 package. This test was chosen as suitable for dealing with non-normal distributions.

RESULTS AND DISCUSSION

As a base for PDT photosensitizer, we used parent N-aminobacteriopurpurinimide, which is highly stable, has peak absorbance at 830 nm, and as was shown in *in vivo* experiments on animal models, exhibits high PDT activity [33]. N-Aminobacteriopurpurinimide was synthesized by reacting bacteriopurpurin **2** with hydrazine hydrate in pyridine according to a known procedure [34]. Bacteriopurpurin was derived via allomerization of BChl *a* **1** accumulated in purple nonsulfur bacterium *Rhodobacter capsulatus* strain B10 grown under chemoheterotrophic conditions following a procedure described in the literature [35-38]. The yield of BChl *a* was 10-14 mg/g dry weight biomass.

Acylation of N-aminobacteriopurpurinimide **3** with lipoic acid in the presence of condensing agent EEDQ (N-carboethoxy-2-ethoxy-1,2-dihydroquinoline) afforded sulfur-containing product **4**, which was further covalently immobilized on gold nanoparticles through the S−Au bond to give nanostructured conjugate **5** (Scheme).

Since bacteriopurpurinimide with the attached lipoic acid moiety **4** is hydrophobic, it was solubilized in

Cremophor ELP, which is an optimal and widely used agent effective at homogenization of poorly water-soluble porphyrin photosensitizers [39].

Photosensitizer **4** was conjugated to gold nanoparticles by stirring its micellar aqueous-Cremophor dispersion with the aqueous solution of NP-Au for 1 day followed by centrifugation and resuspending of the formed PS−Au precipitate in 4% aqueous Cremophor, which allowed separation of gold nanoparticles loaded with photosensitizer (PS−Au, **5**) with 22% yield corresponding to the molar loading ratio of gold nanoparticles (PS **4** loading) as high as 80 PS/PS−Au.

Presence of Q_1 (550 nm) and Q_2 (824 nm) bands in the electronic absorption spectrum of the dispersion confirmed conjugation of the photosensitizer to gold nanoparticles, and monomeric form of immobilized PS **4** is suggested by the characteristic pattern on the spectrum. The signal from NP-Au appears as a shoulder at 520 nm (Fig. 1, spectrum of unloaded NP-Au, dashed line).

Fluorescence of the loaded photosensitizer was used to probe the accumulation of the prepared conjugate PS−Au **5** in the tumor. Irradiation at the wavelength of the Q_1 band excites strong fluorescence at 830 nm due to N-aminobacteriopurpurinimide (Fig. 2), which allowed the assessment of PS and nanoparticles biodistribution.

Gold nanoparticles were synthesized by reducing chloroauric acid with sodium citrate according to the Turkevich method [40]. The procedure yields water-soluble gold nanoparticles capped with a layer of negatively charged citrate ions adsorbed on their surface [41]. The NP-Au and PS−Au **5** nanoparticles were characterized by dynamic light scattering (DLS) (Fig. 3) and transmission electron microscopy (TEM) (Fig. 4) techniques.

As follows from the DLS measurements, the hydrodynamic size of the gold nanoparticles loaded with PS is
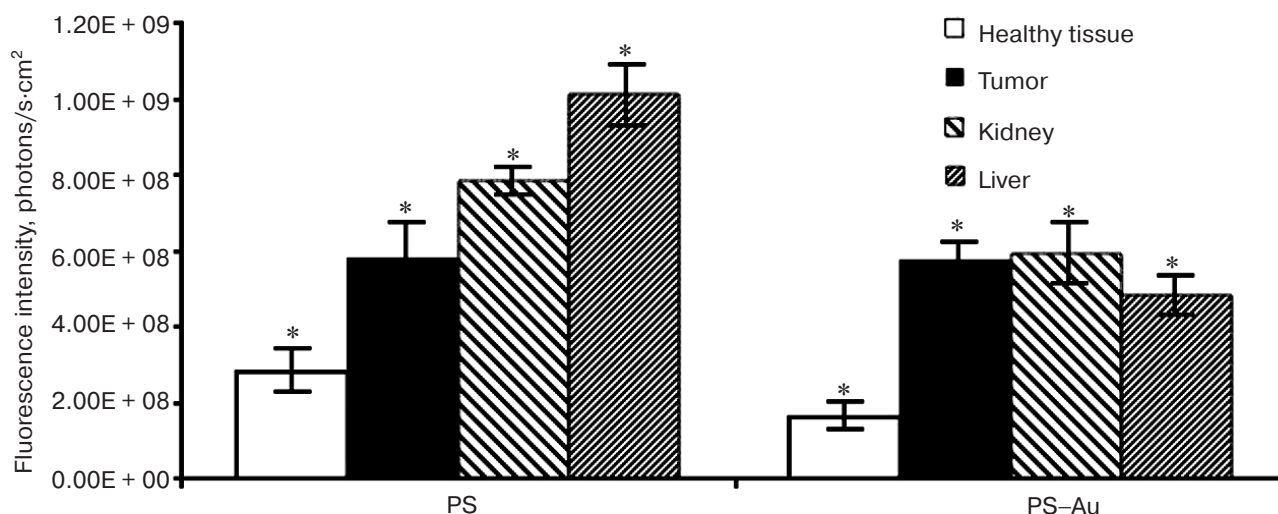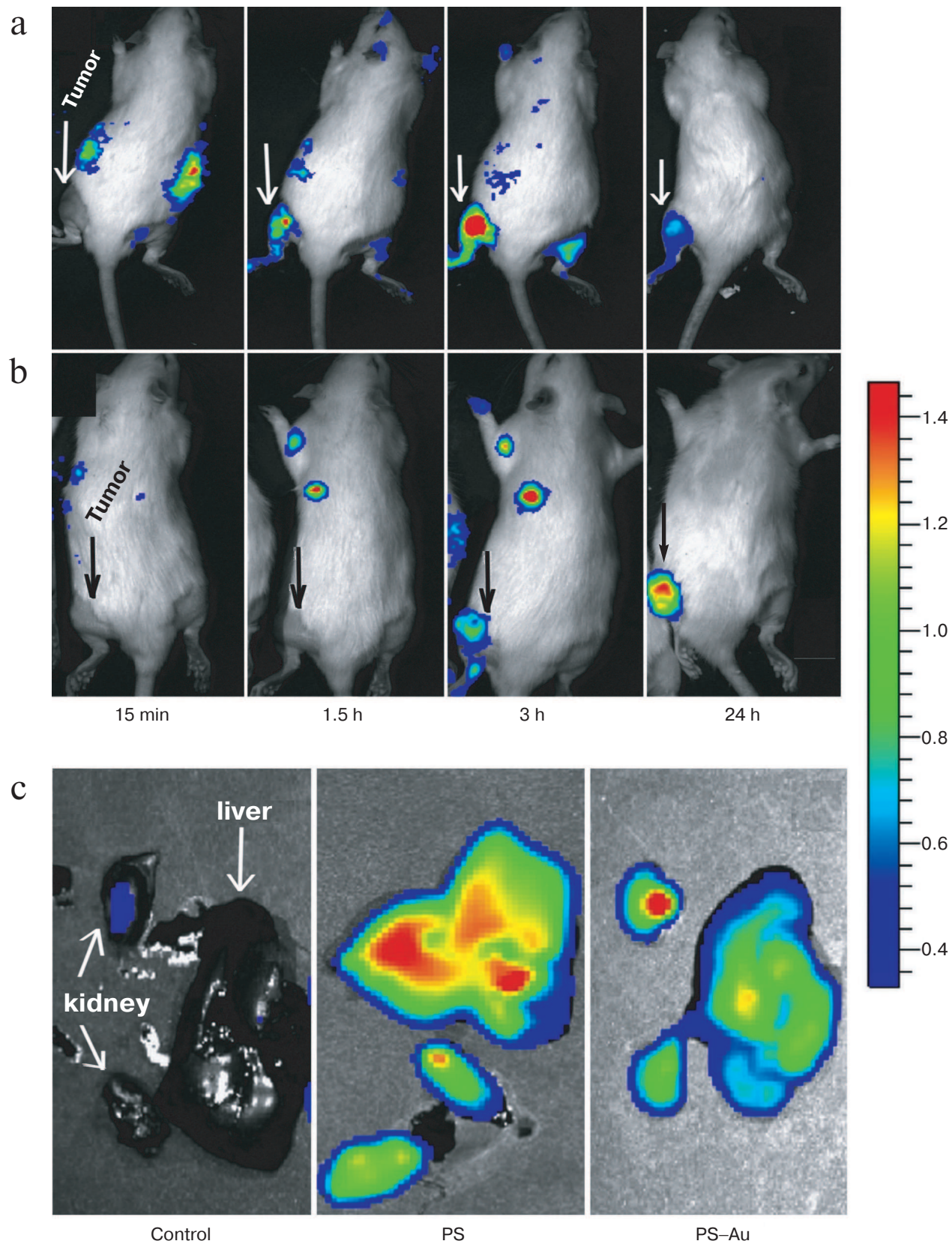

Fig. 7. Normalized fluorescence of photosensitizers PS **4** and PS−Au **5** in the tumor, surrounding tissue, and in liver and kidney at their maximum tumor uptake time points (injection dose 2.5 mg/kg). Each value is the mean of three independent experiments; * $p < 0.05$ (95% confidence).

Fig. 8. Fluorescence imaging of rats bearing sarcoma M-1: *in vivo* images of rats at 15 min, 1.5, 3, and 24 h post injection with PS **4** (a), and rats treated with the immobilized photosensitizer PS−Au **5** (b); *ex vivo* images of kidney and liver at maximum tumor uptake time points for PS **4** and PS−Au **5** (c).

considerably greater than that of the unloaded gold nanoparticles: 10-12 nm for NP-Au vs. 100-110 nm for PS−Au. TEM images (Fig. 4) show some NP aggregates formed after PS immobilization.

The TEM method was used to determine the size and the morphology of the metal core, but this method cannot correctly estimate the size of the organic coating on the surface of the nanoparticles. Thus, the versatile and conventional method of analysis of nano-hybrid materials based on metal nanoparticles, therapeutic agents, and the polymeric stabilizers is the DLS technique. The value of the hydrodynamic radius of the gold nanoparticles obtained by this method indicates the modification of its surface with the organic ligand (lipoic acid) carrying the photodynamic agent and with the Cremophor, which is a stabilizer. Increase of the nanoparticle size is also related to its partial aggregation.

Evaluation of *in vivo* kinetics and biodistribution of free photosensitizer 4 and photosensitizer conjugated to gold nanoparticles 5 in rats implanted with sarcoma M-1. Kinetics and biodistribution of free and immobilized PS were evaluated in *in vivo* studies on ordinary rats obtained from the vivarium of the Medical Radiological Scientific Center (Obninsk) of the Ministry of Health of Russian Federation and kept under standard conditions. The assessment of PS accumulation in the tumor (rat sarcoma M-1) and the surrounding tissue was based on its fluorescence. PS uptake in tissues was estimated from the normalized fluorescence (NF) values. Fluorescence was measured using the local fluorescence spectroscopy (LFS) technique.

As seen from Fig. 5, the conjugation to gold nanoparticles drastically changes the accumulation kinetics of PS in tumor and undamaged tissue. Whereas the maximum tumor uptake of free photosensitizer **4** was achieved at a relatively early time point after administration (210 min; Fig. 5a), the immobilized PS was steadily accumulated during 1 day, reaching its maximum at 24 h (Fig. 5b).

Analysis of the fluorescence contrast (FC) calculated as the ratio of NF in tumor to NF in skin and muscle (Fig. 6, a and b) demonstrated high affinity toward tumor (M-1 sarcoma) for both free photosensitizer **4** and gold nanoparticles loaded with PS (PS−Au **5**). However, the maximum tumor versus skin fluorescent contrast ratios for PS **4** and PS−Au **5** differ and are reached at different post-injection time points: for PS **4**, FC is 2.1 ± 0.3 arb. units at 3.5 h after administration (Fig. 6a), and for PS−Au **5**, FC is 3.2 ± 0.5 arb. units at 24 h (Fig. 6b). After achieving maximum values, normalized fluorescence (NF) of PS **4** and PS−Au **5** in the tumor decreases in similar manner (not shown in Fig. 6). At 72 h post injection, NF in the tumor tissue is decreased by 96-97% from the maximum value. Maximum fluorescence in skin and muscle for compounds **4** and **5** was found at 15 min after administration of PS, and at 72 h post injection, fluorescence is undetectable.

We assessed biodistribution of the free PS **4** and PS−Au **5** in liver and kidney at their maximum tumor uptake time points (210 min for PS **4** and 24 h for PS−Au **5**; Fig. 7). Liver and kidney actively accumulated PS (Fig. 8); expectedly, the tumor-to-tissue fluorescence contrast differs for PS **4** and PS−Au **5**, with the higher affinity to tumor tissue observed in the photosensitizer−gold nanoparticle conjugate.

In this work, tumor visualization was based on fluorescence of PS **4** (Fig. 8a) and its gold nanoparticle conjugate PS−Au **5** in rats bearing M-1 sarcoma (Fig. 8b). As seen from Fig. 8, the dynamics of tumor fluorescence intensity over the 24 h period assessed from fluorescence imaging data agrees with the dynamic behavior of local concentration of PS based on the normalized fluorescence measurement (local fluorescence spectroscopy data obtained with a LESA-6 laser-induced fluorescence spectroscopic system for *in vivo* cancer detection (Biospec, Russia)).

Thus, a combination of fluorescence imaging with *in vivo* local fluorescence spectroscopy was used to demonstrate that the conjugation of the bacteriopurpurinimide-based photosensitizer to gold nanoparticles enhances circulation time of PS in the blood and its tumor uptake due to extravasation of nanoparticles loaded with PS from the circulatory system.

REFERENCES

1. Bonnett, R. (1999) Photodynamic therapy in historical perspective, *Rev. Contemp. Pharmacother.*, **10**, 1-17.
2. Dougherty, T. J., Gomer, C. J., Henderson, B. W., Jori, G., Kessel, D., Korbelik, M., Moan, J., and Peng, Q. (1998) Photodynamic therapy, *J. Natl. Cancer Inst.*, **90**, 889-905.
3. Stranadko, E. F. (2002) Historical development of photodynamic therapy, *Lazer. Med.*, **4**, 4-8.
4. Ronn, A. M. (1999) Pharmacokinetics in photodynamic therapy, *Rev. Contemp. Pharmacother.*, **10**, 39-46.
5. Freitas, I. (1990) Lipid accumulation: the common feature to photosensitizer retaining normal and malignant tissues, *J. Photochem. Photobiol. B*, **7**, 359-361.
6. Mason, M. D. (1999) Cellular aspects of photodynamic therapy for cancer, *Rev. Contemp. Pharmacother.*, **10**, 25-37.
7. Vrouenraets, M. B., Visser, G. W., Snow, G. B., and van-Dongen, G. A. (2003) Basic principles, applications in oncology and improved selectivity of photodynamic therapy, *Anticancer Res.*, **23**, 505-522.
8. Allison, R. R., Downie, G. H., Cuenca, R., Hu, X. H., Childs, C. J. H., and Sibata, C. H. (2004) Photosensitizers in clinical PDT, *Photodiagn. Photodyn. Ther.*, **1**, 27-42.
9. Moan, J., Peng, Q., Iani, V., Ma, L. W., Horobin, R. W., Berg, K., Kongshaug, M., and Nesland, J. M. (1995) Biodistribution, pharmacokinetic and *in vivo* fluorescence spectroscopic studies of photosensitizers, *SPIE*, **2625**, 234-238.

10. Moser, J. G. (1997) Definitions and general properties of 2nd and 3rd generation photosensitizers, in *Photodynamic Tumor Therapy*, *2nd and 3rd Generation Photosensitizers* (Moser, J. G., ed.) Harwood Academic Publishers, London, pp. 3-8.

11. Henderson, B. W., Sumlin, A. B., Owcharczak, B. L., and Dougherty, T. J. (1991) Bacteriochlorophyll *a* as photosensitizer for photodynamic treatment of transplantable murine tumors, *Photochem. Photobiol. B*, **10**, 303-313.

12. Koudinova, N. V., Pinthus, J. H., Brandis, A., Brenner, O., Bendel, P., Ramon, J., Eshhar, Z., Scherz, A., and Salomon, Y. (2003) Photodynamic therapy with Pd-bacteriopheophorbide (TOOKAD): successful *in vivo* treatment of human prostatic small cell carcinoma xenografts, *Int. J. Cancer*, **104**, 782-789.

13. Brandis, A., Mazor, O., Neumark, E., Rozenbach-Belkin, V., Salomon, Y., and Scherz, A. (2005) Novel water-soluble bacteriochlorophyll derivatives for vascular-targeted photodynamic therapy: synthesis, solubility, phototoxicity and the effect of serum proteins, *Photochem. Photobiol.*, **81**, 983-993.

14. Grin, M. A., Mironov, A. F., and Shtil, A. A. (2008) Bacteriochlorophyll *a* and its derivatives: chemistry and perspectives for cancer therapy, *Anti-cancer Agents Med. Chem.*, **8**, 683-697.

15. Mironov, A. F., and Grin, M. A. (2008) Synthesis of chlorin and bacteriochlorin conjugates for photodynamic and boron neutron capture therapy, *J. Porphyrins Phthalocyanines*, **12**, 1163-1172.

16. Peer, D., Karp, J. M., Hong, S., Farokhzad, O. C., Margalit, R., and Langer, R. (2007) Nano-carriers as an emerging platform for cancer therapy, *Nat. Nanotech.*, **2**, 751-760.

17. Ghosh, P., Han, G., De, M., Kim, C. K., and Rotello, V. M. (2008) Gold nanoparticles in delivery applications, *Adv. Drug Delivery Rev.*, **60**, 1307-1315.

18. Rana, S., Bajaj, A., Mout, R., and Rotello, V. M. (2012) Monolayer coated gold nanoparticles for delivery applications, *Adv. Drug Delivery Rev.*, **64**, 200-216.

19. Dreaden, E. C., Alkilany, A. M., Huang, X., Murphy, C. J., and El-Sayed, M. A. (2012) The golden age: gold nanoparticles for biomedicine, *Chem. Soc. Rev.*, **41**, 2740-2779.

20. Bardhan, R., Lal, S., Joshi, A., and Halas, N. J. (2011) Theranostic nano-shells: from probe design to imaging and treatment of cancer, *Acc. Chem. Res.*, **44**, 936-946.

21. Xia, Y., Li, W., Cobley, C. M., Chen, J., Xia, X., Zhang, Q., Yang, M., Cho, E. C., and Brown, P. K. (2011) Gold nanocages: from synthesis to theranostic applications, *Acc. Chem. Res.*, **44**, 914-924.

22. Cheng, Y. C., Samia, A., Meyers, J. D., Panagopoulos, I., Fei, B., and Burda, C. (2008) Highly efficient drug delivery with gold nanoparticle vectors for *in vivo* photodynamic therapy of cancer, *J. Am. Chem. Soc.*, **130**, 10643-10647.

23. Cheng, Y., Samia, A. C., Li, J., Kenney, M. E., Resnick, A., and Burda, C. (2009) Delivery and efficacy of a cancer drug as a function of the bond to the gold nanoparticle surface, *Langmuir*, **26**, 2248-2255.

24. Cheng, Y., Meyers, J. D., Broome, A.-M., Kenney, M. E., Basilion, J. P., and Burda, C. (2011) Deep penetration of a PDT drug into tumors by noncovalent drug-gold nanoparticle conjugates, *J. Am. Chem. Soc.*, **133**, 2583-2591.

25. Srivatsan, A., Jenkins, S. V., Jeon, M., Wu, Z., Kim, C., Chen, J., and Pandey, R. K. (2014) Gold nanocage−photosensitizer conjugates for dual-modal image-guided enhanced photodynamic therapy, *Theranostics*, **4**, 163-174.

26. Mieszawska, A. J., Mulder, W. J. M., Fayad, Z. A., and Cormode, D. P. (2013) Multifunctional gold nanoparticles for diagnosis and therapy of disease, *Mol. Pharm.*, **10**, 831-847.

27. Galper, M. W., Saung, M. T., Fuster, V., Roessl, E., Thran, A., Proksa, R., Fayad, Z. A., and Cormode, D. P. (2012) Effect of computed tomography scanning parameters on gold nanoparticle and iodine contrast, *Invest. Radiol.*, **47**, 475-481.

28. Liu, C. J., Wang, C. H., Chen, S. T., Chen, H. H., Leng, W. H., Chien, C. C., Wang, C. L., Kempson, I. M., Hwu, Y., Lai, T. C., Hsiao, M., Yang, C. S., Chen, Y. J., and Margaritondo, G. (2010) Enhancement of cell radiation sensitivity by pegylated gold nanoparticles, *Phys. Med. Biol.*, **55**, 931-945.

29. Chen, X., Chen, Y., Yan, M., and Qiu, M. (2012) Nanosecond photothermal effects in plasmonic nanostructures, *ACS Nano*, **6**, 2550-2557.

30. Chen, H., Shao, L., Ming, T., Sun, Z., Zhao, C., Yang, B., and Wang, J. (2010) Understanding the photothermal conversion efficiency of gold nanocrystals, *Small*, **6**, 2272-2280.

31. Huang, X., Kang, B., Qian, W., Mackey, M. A., Chen, P. C., Oyelere, A. K., El-Sayed, I. H., and El-Sayed, M. A. (2010) Comparative study of photothermolysis of cancer cells with nuclear-targeted or cytoplasm-targeted gold nanospheres: continuous wave or pulsed lasers, *J. Biomed. Opt.*, **15**, 058002.

32. Mironov, A. F., Kozyrev, A. N., and Brandis, A. S. (1992) Sensitizers of second generation for photodynamic therapy of cancer based on chlorophyll and bacteriochlorophyll derivatives, *Proc. SPIE*, **1922**, 204-208.

33. Mironov, A. F., Grin, M. A., Tsiprovskiy, A. G., Dzardanov, D. V., Golovin, K. V., Feofanov, A. V., and Yakubovskaya, R. I. (2004) Bacteriochlorophyll *a*-based hydrazides possessing photodynamic activity and method for their preparation, Patent RF 2223274 [in Russian].

34. Mironov, A. F., Grin, M. A., Tsiprovskiy, A. G., Kachala, V. V., Karmakova, T. A., Plyutinskaya, A. D., and Yakubovskaya, R. I. (2003) New bacteriochlorin derivatives with a fused N-aminoimide ring, *J. Porphyrins Phthalocyanines*, **7**, 725-730.

35. Mironov, A. F., and Efremov, A. V. (1996) Synthesis of bacteriochlorophyll *a*, Patent RF 2144085 [in Russian].

36. Tsygankov, A. A., Laurinavichene, T. V., and Gogotov, I. N. (1994) Laboratory scale photobioreactor, *Biotechnol. Tech.*, **8**, 575-578.

37. Tsygankov, A. A., Laurinavichene, T. V., Bukatin, V. E., Gogotov, I. N., and Hall, D. O. (1997) Biomass production by continuous cultures of *Rhodobacter capsulatus* grown in various bioreactors, *Biochem. Microbiol.*, **33**, 485-490.

38. Patrusheva, E. V., Fedorov, A. C., Belera, V. V., Minkevich, I. G., and Tsygankov, A. A. (2007) Synthesis of bacteriochlorophyll *a* by the purple nonsulfur bacterium *Rhodobacter capsulatus*, *Appl. Biochem. Microbiol.*, **43**, 187-192.

39. Sharonov, G. V., Karmakova, T. A., Kassies, R., Pljutinskaya, A. D., Refregiers, M., Yakubovskaya, R. I., Mironov, A. F., Grin, M. A., Maurizot, J.-C., Vigny, P., Otto, C., and Feofanov, A. V. (2006) Cycloimide bacteriochlorin *p* derivatives: photodynamic properties, cellular and tissue distribution, *Free Radicals Biol. Med.*, **40**, 407-419.

40. Turkevich, J., Stevenson, P. C., and Hillier, J. (1951) A study of the nucleation and growth processes in the synthesis of colloidal gold, *Discuss. Faraday Soc.*, **11**, 55-75.

41. Frens, G. (1973) Controlled nucleation for regulation of particle size in monodisperse gold suspensions, *Nat. Phys. Sci.*, **241**, 20-22.